Ultrasonics 65 (2016) 200–210

Contents lists available at ScienceDirect

Ultrasonics

journal homepage: www.elsevier.com/locate/ultras

Induction coil as a non-contacting ultrasound transmitter and detector: Modeling of magnetic fields for improving the performance

Dirk Rueter *

University of Applied Sciences Ruhr West, 45473 Muelheim, Germany

ARTICLE INFO

Article history:
Received 14 November 2014
Received in revised form 2 June 2015
Accepted 2 October 2015
Available online 22 October 2015

Keywords:
EMAT modeling
Increased liftoff
High power

ABSTRACT

A simple copper coil without a voluminous stationary magnet can be utilized as a non-contacting transmitter and as a detector for ultrasonic vibrations in metals. Advantages of such compact EMATs without (electro-)magnet might be: applications in critical environments (hot, narrow, presence of iron filings...), potentially superior fields (then improved ultrasound transmission and more sensitive ultrasound detection).

The induction field of an EMAT strongly influences ultrasound transduction in the nearby metal. Herein, a simplified analytical method for field description at high liftoff is presented. Within certain limitations this method reasonably describes magnetic fields (and resulting eddy currents, inductances, Lorentz forces, acoustic pressures) of even complex coil arrangements. The methods can be adapted to conventional EMATS with a separate stationary magnet.

Increased distances (liftoff) are challenging and technically relevant, and this practical question is addressed: with limited electrical power and given free space between transducer and target metal, what would be the most efficient geometry of a circular coil? Furthermore, more complex coil geometries ("butterfly coil") with a concentrated field and relatively higher reach are briefly investigated.

1. Introduction

Magnetic fields are utilized in electromagnetic acoustic transducer (EMAT) schemes for ultrasound excitation and detection in metallic test objects [1]. The application is ultrasound testing of metallic work pieces with a non-contacting and non-destructive method. As an inherent advantage the magnetic fields permeate most dielectric barriers (air, humidity, dirt, plastic foil...) and exclusively interact with the metallic target.

A practical disadvantage is that the achieved transduction efficiencies and ultrasound intensities are quite modest with respect to contacting PZT transducers. The efficiency even strongly decreases with increasing gap (=liftoff g) between the metal surface and EMAT; therefore, in practical applications, the g is usually smaller than a few mm.

Conventional EMATs consist of an RF inductor coil and a permanent magnet. The permanent magnet projects a DC magnetic flux density B_0 toward the target metal. The RF inductor induces eddy currents in the metal surface, and together with B_0, Lorentz forces or pressures at RF frequencies are experienced in the metal, resulting into ultrasound transduction. A conventional EMAT with permanent magnet also works as an ultrasound detector.

The conversion efficiency between electrical excitation power and achieved ultrasound intensity scales with the locally (at and in the metal surface) present B_0^2 [2], which is proportional to the local energy density of the permanent field B_0. Also the sensitivity of an EMAT as an ultrasound detector scales with B_0^2. On the basis of conventional magnets, it is quite difficult to achieve magnetic flux densities toward or even higher than 1 T over certain distance g into the metal target. Practically very relevant, this limits the conversion efficiency, the overall sensitivity and, in particular, the effective range of EMAT techniques.

In an even simpler transmitter scheme, an RF induction coil alone—without a permanent magnet—can also excite ultrasound vibrations in a distant metallic target. Here, the dynamic field B_{RF} from the induction coil (at RF frequencies), together with the induced eddy current (being proportional to the dynamic field B_{RF}), produces RF Lorentz forces and ultrasonic vibration [3–8]. Therefore, the Lorentz forces or effected RF pressures are proportional to ${B_{RF}}^2$. It has been known for a long time [3,4,8] that this quadratic relation has several consequences: the Lorentz forces and pressures are exclusively repulsive (unipolar), and they oscillate with a doubled RF frequency. In addition, the dynamic field B_{RF} cannot permeate into the depth of the metal target. Thereby

* Tel.: +49 1606321020.
E-mail address: dirk.rueter@hs-ruhrwest.de

http://dx.doi.org/10.1016/j.ultras.2015.10.003
0041-624X/

the in-plane field component of a dynamic field is increased with respect to a stationary field with same excitation currents. This field deformation ("field compression") influences the Lorentz forces: the out-of-plane forces are increased and the in-plane forces are reduced with respect to a conventional EMAT with stationary field. It can be shown (paragraph 7 in the supplement) that with a limited amount of total magnetic energy (energies of stationary and dynamic field together) the achieved ultrasound intensity with just an RF field and without a stationary field is actually maximal. It is however a practical problem to provide high magnetic energies at RF frequencies. Undoubtedly, a strong NdFeB permanent magnet with just a "cold" DC field is more convenient.

Without stationary magnet, the excited ultrasound intensity scales with the square of the RF pressures and is proportional to $B_{RF}{}^4$. In other words, the excited ultrasound power increases with the square of the electrical power in the RF induction coil. The relation holds as long as the excited ultrasonic power is much smaller than the electrical power and this restriction is usually fulfilled: the conversion efficiency for MHz ultrasound typically is much lower than 1%.

With sufficiently high excitation power, a simple induction coil can provide magnetic flux densities B_{RF} significantly above 1 T, more than the stationary field in a conventional EMAT. In addition, as inherent advantage, the B_{RF} implicitly displays geometrical overlap with the induced eddy currents in the target metal. Thus, relatively high acoustic pressures are achieved and relatively strong ultrasound signals can be transmitted [3,9].

It is repeatedly noted as a substantial weakness of a "coil only EMAT" without an additional and stationary field that it cannot detect ultrasound vibrations [3,4,6,8]. This is true for a *passive* coil. The problem can be overcome by using an *active* coil as a *receiver* and this concept is briefly demonstrated here. It should however be noticed that this topic is not intended as the main purpose of this contribution, nor shall this demonstration be understood as a fully developed design.

Fig. 1 describes an experimental proof of concept for ultrasound transmission and ultrasound detection via two non-contacting "coil only EMATS". Two practically identical spiral coils L_1 and L_2 with 5 windings each were made from 1 mm copper wire. The outer radius of the spirals is 20 mm. No ferromagnetic material or permanent magnet is involved. The central element is an aluminum rod (70 cm length, 20 mm diameter), which serves as a delay line for an ultrasound transmission. In such basic experiments, a defined delay is helpful for a clear separation between initial signal artifacts and true ultrasonic signals. The coils are positioned close – but non-contacting – to the plane endings of the aluminum rod; the air gap g between coils and rod is chosen to approximately 1 mm.

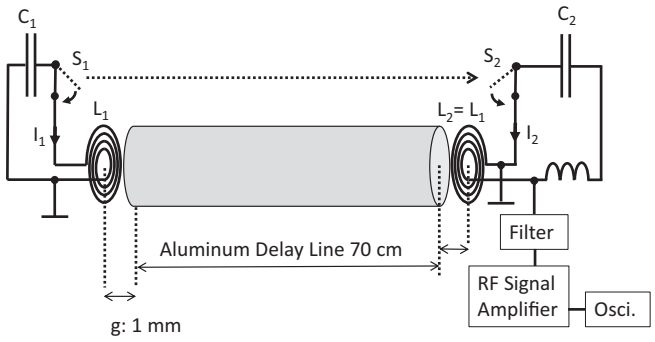

Fig. 1. Two identical coils L_1 and L_2 ("copper only") are demonstrated as contactless ultrasound transmitter (left arrangement, similar to [9]) and ultrasound detector (right arrangement) at MHz frequencies. For ultrasound detection, L_2 is activated with a strong and relatively prolonged (typ. 1 ms) current pulse I_2 from C_2. The detected signal (MHz) then can be tapped from L_2. Potentially stronger fields with a more suitable topology can be achieved for the detector L_2.

The capacitor C1 is charged to 12 kV and, when switch S_1 fired, a pulsed and strong RF current I_1 excites the inductor L_1, well approaching 10 kA for a few µs. This scheme transmits a strong ultrasonic pulse into the delay line, as already described in much more detail and readily available for the interested reader [9]. Here the frequency of the LC-circuit L_1 and C_1 was 700 kHz and thus, the characteristic frequency of the transmitted ultrasound was 1.4 MHz.

The coil L_2 at the other ending of the delay line is connected to a similar circuitry. The solid state switch S_2 (an IGBT battery) is instantaneously triggered by S_1 or I_1. Then capacitor C_2 starts to discharge into L_2. C_2 is chosen much bigger (35,000 µF) than C_1 (150 nF) and the voltage is much lower (25 V). Therefore the discharge current I_2 rises much slower (≈100 µs) and lasts much longer (≈1 ms) than I_1. From the discharge characteristics it can be derived that the magnitude of I_2 approaches 2 kA. Then L_2 produces a magnetic flux density (compare [9], more calculus below) within the gap g in the order of 2 T. This is stronger than available from even voluminous permanent magnets and furthermore, that field from L_2 is spatially matched to the eddy current sensitivity of L_2. The pulsed L_2 clearly repels metals (magnetic pressure), even ferromagnetic iron and steel is rejected. Only non-conducting and ferromagnetic material (ferrite, iron powder cores) is attracted by L_2.

During this relatively long current pulse I_2 an additional RF signal can be tapped from L_2. That RF signal was guided through a simple filter element and – after some impedance transformation and amplification – was available for the oscilloscope.

Clearly an RF burst after 110 µs and at about 1.4 MHz is observed in the oscilloscope. 110 µs equals the traveling time of sound through the 70 cm aluminum rod. That RF signal at 1.4 MHz strongly decreases, when either retracting L_1 or L_2 from the aluminum endings. An additional echo after 340 µs (ultrasound pulse traveling for, back, and for again) is observable. The signals are quite similar to those already presented in [9] and besides multiple echoes, also distinct longitudinal propagation modes from the aluminum rod are observable [9,10]. The signal's raw amplitude – before amplification – was about 40 mV and this is not a small effect for an EMAT. The observed 1.4 MHz signal completely disappears when suppressing I_2.

The signal amplitude is proportional to I_2, or: the signal energy at a given ultrasonic vibration (=conversion efficiency) is proportional to the field energy B^2, as in conventional EMATs. The *transmitted* ultrasound from the L_1 (left) however scales with B^4 [3,4,9]. There is a difference between transmitting and receiving ultrasound. Nevertheless, it is out of the question that the activated L_2 as a "copper only EMAT" has become a non-contacting detector for MHz ultrasound.

When – instead of releasing the pulsed current I_2 – attaching a reasonably shaped NdFeB permanent magnet to the back side of L_2, the detector coil works like a conventional EMAT with a static field. Then however, in direct comparison, the received signal amplitude is notably weaker: instead of 40 mV with I_2 only 6 mV is obtained with the NdFeB magnet. Although the NdFeB design certainly could be more optimized, it is not likely that the principal efficiency of the "copper only" system L_2 and I_2 as a *detector* (which also can be more optimized) can be reached with such separate and conventional magnet: the inherent advantage of the "copper only system" is the geometrical match between excitation field and sensing of eddy currents, together with stronger magnetic fields. An additional enhancement – besides an optimized coil geometry and strong I_2 – could be achieved by a ferrite back plate [7] or perhaps by an iron powder back plate (higher saturation toward ≈ 2 T). Such back plates are not intended as permanent magnets but they

help to reduce unnecessary magnetic energy at the inductor's back side. Then relatively more energy is available at the front side and the sensitivity is increased.

Instead of a prolonged unipolar current pulse I_2, also a strong RF burst (with frequency f_2) could be used for the activation of L_2. In general, the receiver system behaves as an RF mixer, i.e. the output signal is a multiplicative product of two input signals (ultrasound at frequency f_1 and I_2 at f_2). Then the interesting output signal of the mixer would be situated at the sum $(f_1 + f_2)$ and the difference frequency $(f_1 - f_2)$. In the above described experiment f_2 was almost zero with respect to f_1, thus the frequency of the output signal was virtually unchanged. Frequency mixing is almost regularly used in sensitive and selective RF receivers. An additional advantage of an RF pulse I_2 would be a distinct compression and enhancement of an RF magnetic field (see below and supplement). This beneficial effect does not occur for relatively slow or even DC fields: those will expand and dilute into the metal target.

Echo operation would require a single coil as a powerful emitter and as a sensitive receiver for MHz ultrasound at (almost) the same time. This is currently not demonstrated, but probably will be seen in the near future.

The relative high currents (kA) and voltages (kV for the transmitter) were chosen for better signal levels in this principal demonstration. At higher repetition rates, such energetic pulses would heat up the coils to critically high temperatures. This would limit or even prevent many practical applications. However, at somewhat reduced voltages and currents and with cooling measures (e.g., by forced air) the repetition frequencies can exceed 10 Hz [9] or even 100 Hz, much more suitable for many industrial applications. Reasonably reduced voltages and powers also would considerably relieve the challenge for a maintenance free all-solid-state design.

Nevertheless, the efficiency of the above described (Fig. 1) signal transmission is still very poor and this is a general and practically relevant weakness of EMATs. A raw estimation for the overall efficiency is obtained by the ratio of squared signal amplitudes: $\eta \approx (40\ \mathrm{mV})^2/(12\ \mathrm{kV})^2 \approx 10^{-11}$. An optimized signal transmission with two *contacting* PZT transducers certainly would perform very much better (η might exceed 10^{-1}).

An important key for gradually increasing the efficiency of non-contacting EMATs is the understanding and control of magnetic field topologies. In general, magnetic fields demand energy or electrical power (the dynamic fields). The limited energy or power in EMAT systems preferably should be used for those magnetic fields near the target surface. Fields apart from the target just demand additional energy, but they do not contribute for electroacoustic coupling and then decrease the overall efficiency.

The energy density p of a magnetic field is known as

$$p = \frac{\mu}{2} B^2 \tag{1}$$

At the same time this energy density is equivalent to the *magnetic pressure p*. p readily manifests as a mechanical pressure on a metal surface when it is exposed to a transient magnetic field (supplement). An oscillating mechanical pressure can be utilized for ultrasound transmission. The magnetic pressure at the target site is proportional to the electroacoustic conversion efficiency [2] of an EMAT emitter and receiver, as already stated above with the "copper only receiver".

While the calculus based on magnetic pressure p is relatively convenient, a discrete handling of the magnetic fields diffusing into the skin sheet δ of the metal, induced eddy current fields in the skin sheet, and resulting Lorentz forces in the skin volume would also ultimately yield the same results for relatively high liftoff distances (supplement). Then it can be shown that the magnetic or mechanical pressure p is virtually independent from the metal type. The restriction is however that the characteristic size of the field, here given by the liftoff g, should be much higher than the characteristic skin depth δ of the metal (supplement, for example, $g \geqslant 10\delta$). Additionally, higher liftoff distances (say $g \geqslant 1$ mm) are practically very interesting. This condition is explicitly addressed here.

In previous experiments [9], metallic targets were exposed to relatively high magnetic flux densities of up to 10 T from a flat spiral coil (left part of Fig. 1). The coil was excited with a pulsed RF current of more than 10 kA at a 1 MHz oscillation frequency. The amplitude of the magnetic (or mechanic) pressure was found to be about 400 atmospheres (experimental result in [9] and Eq. (1)), and that pressure oscillated with doubled frequency, thus generating a considerable ultrasound pulse (up to kW levels) at 2 MHz in the aluminum target.

The experimental findings at relatively small gaps g (small is 1 mm here) between a flat spiral coil and a metal target were found to be in reasonable accordance with a simplified theoretical description [9] based on some approximations: about 50–70% of the total magnetic energy of the flat spiral coil with a sufficiently large radius ($R > 5\ g$) can be assumed to be fairly homogeneously distributed within the volume of gap g. The characteristic energy density in the gap volume is determined from the total electrical energy in the system—well accessible via electrical measurement—and should equal the oscillating pressure p on the metal as the actual ultrasound source.

Although it reasonably describes the previously observed phenomena, it is recognized that such a simplified theory cannot properly describe situations with relatively *wider gaps* (coil radius $R < 5\ g$). However, such increased distances between the metal target and the transmitter are of particular interest for a non-contacting method.

As the gap increases, the magnetic field in the gap is not at all homogeneous (as assumed in the previous description), but rather, it tends to concentrate around the coil. As a result, the electroacoustic conversion displays a sharp decrease, much greater than as predicted by the simplified description.

Due to the nonlinear mechanism of this transducer scheme, at small liftoff g, a smaller coil with higher energy *density* (=pressure) is more effective for ultrasound generation than a larger coil with the same electrical energy [9]. In both cases, the affected *forces* on the metal are almost equal, but the *pressures* are higher for the smaller coil: acoustic power transduction scales with the square of pressure.

On the other hand, at increased distances g, the larger coil, with its wider field extension, is more effective than a smaller coil with less range. Apparently, an optimum radius R of the inductor should exist for each distance g. This question will be addressed below.

Even a quite idealized scenario is not satisfied by just two geometries (a gap g and a radius R of the inductor coil): as an additional and basic geometry, an active width or filling f of the coil can be introduced (Fig. 2a), with $0 < f < R$. It can be expected that this filling will also influence the pressure effects and sound efficiency.

Within the active filling f, the optimum design rule of a flat spiral coil is quite clear: the individual windings should be as wide as possible in the radial direction to avoid an unnecessary magnetic field (and energy) concentration at the windings. The windings should leave just enough radial gaps for insulating the neighbor windings against an RF breakdown. The potential difference can be considerably high, in previous experiments up to several kV to the nearest neighbor.

For a potential optimization of induction coils as ultrasound transducers, particularly at increased liftoff distances g, it is the purpose of this contribution to investigate the magnetic field topologies and the associated phenomena in more detail.

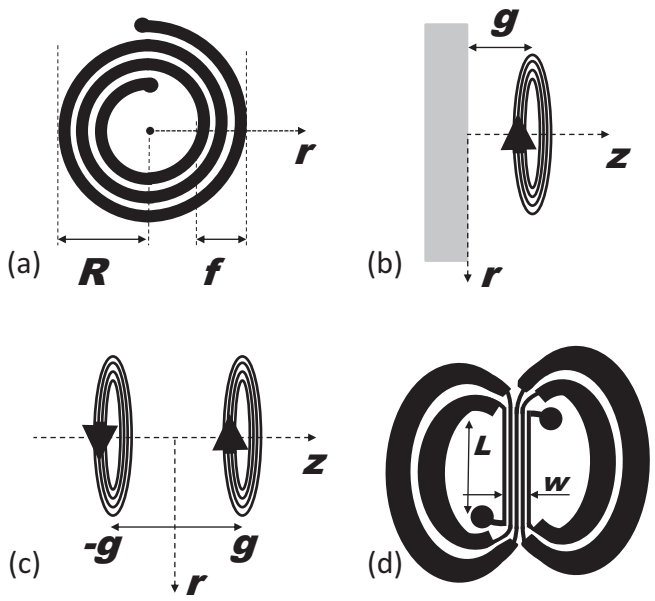

Fig. 2. (a) Flat spiral coil ("pancake coil") with outer diameter R and active filling f. (b) The application is modeled as a number of concentric current circles placed over a metal plane at distance g. (c) Instead of a metal plane, a virtually identical field distribution in the right half space is obtained with a mirror coil with the same geometries and opposite current direction. (d) An alternative and more complex geometry ("butterfly coil") consists of a concentrated (inner) part with high field densities and wider back wings (outside) with low field concentration.

A rigorous solution for calculating the magnetic vector potential from circular current loops in vicinity to metals was presented by Dodd and Deeds [11]. The solution for the free space above the metal surface and within the metal was given in terms of integrals of Bessel functions. With the known vector potential, all relevant field components and eddy currents in and above the metal are available. These can be used for an accurate calculation of the total inductivity and also for Lorentz forces in the metal, e.g., for description and optimization of EMATs, as shown by Jian and Dixon [7] or Kawashima [12]. The method is also exact for small liftoff distances, say 0.2 mm [7]. The mathematical approach and the effort for a software implementation is however not negligible. Many engineers would prefer more convenient FEM simulation tools or a more lucid and handy analytical description.

Here a simplified analytical approach for fields from current loops over a metal plane is presented. It provides accurate field descriptions under the restriction, that the skin depth δ of the metal is relatively small with respect to the gap g between coil and metal plane ($g \geqslant 10\ \delta$). This restriction is reasonably fulfilled for $g \geqslant 1$ mm and MHz frequencies. In aluminum metal, the characteristic skin layer δ is about 80 µm at 1 MHz, which is sufficiently small with respect to a gap g of 1 mm (or more). An acoustic wavelength at 2 MHz in aluminum is in the order of 3.2 mm. For the calculation a real metal with finite conductivity then can be replaced – without very much influencing the interesting fields – by an ideal metal with infinite conductivity (supplement).

Within the limited scope of this distribution (i.e., a relatively wide gap g), the finite conductivity of coil windings and target metals will not be investigated in further detail. As observed in a previous work [9], the finite conductivity of a coil and metallic target will not significantly affect the magnetic pressure and the associated phenomena for a given excitation current. Then the experienced force and pressure was observed as practically the same for quite different and even ferromagnetic metals, namely equal to the magnetic energy density in the gap. Indeed, this experimental observation was made with a relatively wide gap ($g \approx 1\ \text{mm} \gg \delta$). Due to the relative weak coupling over distance, the metal will absorb more or less energy over time, thereby attenuating the magnetic energy within several oscillation periods of the pulsed signal (=some µs at MHz frequencies).

For a single, ideal current loop with radius R and current I, centered in free space (magnetic field constant μ_0) at $z = 0$ and $r = 0$, an analytical solution for the magnetic field components in r-direction (B_r) and z-direction (B_z) exists. The formulas, which are useful but are not very often found in the literature, are from [13]:

$$B_r(r,z) = \frac{\mu_0 I z}{2\pi r}\sqrt{\frac{m}{4Rr}}\left(\frac{2-m}{2-2m}E - K\right) \tag{2a}$$

$$B_z(r,z) = \frac{\mu_0 I}{2\pi r}\sqrt{\frac{m}{4Rr}}\left(rK + \frac{Rm-(2-m)r}{2-2m}E\right) \tag{2b}$$

$$m = \frac{4Rr}{(z^2+(R+r)^2)} \tag{2c}$$

The functions $E(m)$ and $K(m)$ are complete elliptic integrals of the first kind (K) and second kind (E); the numerical data can be found in mathematical table collections. More interestingly, these functions can also be used in mathematical software tools. Thus, the magnetic field from a single current loop or from several current loops (then components just superimposed) can be well modeled in space.

When approaching (Fig. 2b) a single current loop to a conducting metal block ($g \geqslant 10\ \delta$), an almost exact analytical solution for the *dynamic field* (not for a *stationary field* from DC current, this can permeate into the metal) is obtained by additionally introducing a *mirrored* current loop instead of the metal. This is a fairly common strategy for solving such problems in electrodynamics (Fig. 2c). The mirrored loop has the same, but mirrored, geometries and a contra-directional current, and it is centered at $z = -g$. Then, the field distribution (local energy densities, total energy) of the interesting half space becomes identical to the problem of an ideal metal plane at $z = 0$. For example, all B_z components are nulled at $z = 0$, and the B_r components are doubled. Actually, from exact solutions with real metals [11] the B_z components from dynamic fields at $z = 0$ are relatively small for scenarios with $g \gg \delta$. The doubling of the B_r component is an appreciated feature of dynamic fields ("field compression"). This doubling does not occur for a static field, which can expand into a metal. No mirror coil is needed for a description of stationary fields from a current loop over non-magnetic ($\mu_r = 1$) metals. Fields from permanent magnets can be modeled in that way. Additionally, stationary fields over ferromagnetic ($\mu_r \gg 1$) metals could also be readily modeled with mirror coils (in principle, just parallel instead of contra-directional currents in the mirror loops) but shall not be discussed here in more detail.

The influence of mirrored loops can be included (=superimposed) in the calculation by repeatedly using Eq. (2). More complex coil geometries over a metal can be obtained by superimposing more current loops and their mirrors.

The effort for software implementation of this straight forward method is lower than for the more general solution from [11]. As already noted, this method delivers quite accurate fields B_r and B_z for eddy current scenarios with $g \gg \delta$. The azimuthal sheet current density JS_φ at the surface (which then represents and replaces the complex eddy current density in the volume of real metals, see supplement) for non-magnetic metals just becomes

$$JS_\varphi(r) = \frac{B_r}{\mu_0} \tag{3a}$$

and a normally directed surface pressure – directly suitable for ultrasound transmission – is then

$$p_z(r) = JS_\varphi(r) * \frac{B_r}{2} = \frac{B_r^2}{2\mu_0} \tag{3b}$$

which is identical to the energy density of the field at the metal surface or the magnetic pressure (Eq. (1)). A factor of 1/2 results from the average of full B_r directly above the JS_φ and nulled B_r directly below JS_φ. 1/2 is also the exact solution from more detailed analysis (supplement).

As already stated, for an efficiency optimization of an ultrasound transducer the magnetic energy at the surface sheet (Eq. (3b)) should be maximized in relation to the totally available magnetic energy of the EMAT.

The total magnetic field energy E_M of a single loop or several superimposed current loops is obtained by integrating the magnetic energy density (Eq. (1)) of the field (Eq. (2)), including mirror fields, over the half space above the metal plane:

$$\begin{aligned} E_M &= \int_{z=0}^{\infty}\int_{r=0}^{\infty} p(r,z)2\pi r\, dr\, dz \\ &= \int_{z=0}^{\infty}\int_{r=0}^{\infty} \frac{\mu_0}{2}\left(B_r^2 + B_z^2\right)2\pi r\, dr\, dz \end{aligned} \tag{4}$$

For a mathematical current loop, field B becomes infinite (in Eq. (2)) at the current thread at $r = R$ and $z = 0$. As a mathematical consequence, Eq. (4) then also would become infinite. This is however not a problem in a practical and numerical application of these expressions: the relative high or diverging B values in proximity to the current threads can just be omitted (=set to zero within a certain proximity to the ideal current line, e.g., closer than 0.5 mm), and then an integration (Eq. (4)) yields a finite magnetic energy E_M. Indeed, the magnetic field (and energy) inside a 1 mm copper wire at RF frequencies is almost zero; it does not diverge at all.

Furthermore, a numerical integration of E_M just needs to be carried out over a finite volume around the inductor (a limited volume in the r- and z-directions, about 2 times R). Very most of the field energy is allocated closely around an air coil; it does not extend very far into space.

In general, the total magnetic energy of an inductor L is also known as

$$E_M = \frac{1}{2} L I^2 \tag{5}$$

and when comparing Eqs. (5) and (4), the inductance L of a coil, in an even more complex arrangement of several concentric or coaxial windings over a metal plane, can be computed, yielding reasonable results. The energy field (=magnetic pressure) of such a coil can be determined by Eqs. (2) and (1).

One of the optimization criteria for an EMAT is certainly the electroacoustic conversion efficiency: with a given distance g and limited power or limited electrical energy in the inductor, a maximum sonic pressure ($\sim B^2$) or total acoustic power A (comes below with Eq. (6)) at the distant target site is desired. The only influence for such optimization is the inductor's geometry. Ferromagnetic materials become saturated and cannot assist anymore at high fields >2 T (which are anticipated here). The coil windings determine the magnetic field topology, and thus, the intensity and distribution of pressure at the target plane.

The transmitted acoustic power A in the metal is approached by an integration of acoustic power densities over the surface. Again, instead of a much more detailed and complex analysis of acoustic fields [12], a gradually simplified approximation under certain restrictions is made: for dynamic fields, the out-of-plane forces in z – direction are clearly dominating (supplement). The excitation of radial (in-plane) forces as a source for acoustic energy is, therefore, neglected. Secondly, the spatial dimensions of the pressure field onto the surface (since $g > 1$ mm and the typical coil radius $R \gg 1$ mm) are notably wider than a half acoustical wavelength at MHz – frequencies. Therefore, most acoustic energy is provided as a longitudinal elastic wave and this is preferably directed normally into the depth of the metal (z-direction). At low MHz frequencies and small coil sizes not just a plane wave is generated. A much more complex acoustic field with a characteristic structure and opening angle [12,14,15] is emitted and such acoustic field undergoes multiple lateral reflections in a rod (Fig. 1), finally resulting in a longitudinal mode structure [9,10] with multiple replicas (not talking about echoes over the length of the rod) in the received signal. For higher frequencies and relatively much shorter wavelengths however, the acoustic field would gradually approach a longitudinal plane wave. Then, for an EMAT with an exclusively dynamic field, the acoustic power density over the surface scales with the square of magnetic pressure p at $z = 0$ (at the metal plane) and the total power transportation of a longitudinal plane wave would be:

$$A = \int_{r=0}^{\infty} \frac{p(r)^2}{8Z_M} 2\pi r\, dr \tag{6}$$

Z_M is the acoustic impedance of the target metal (aluminum: $Z_M \approx 17 \cdot 10^6$ N s/m^3), and the 8 results from a 2 (p is the peak pressure instead of the mean effective pressure) and a 4 (the unipolar peak pressure from the magnetic field must be halved into positive and negative acoustic peak pressures). Herein, Eq. (6) is used as an approximation for the acoustic power A, even for lower frequencies and then without a plane wave characteristics. For an efficiency optimization in a "copper only transmitter", the transmitted acoustical power A should be maximal for a given E_M (Eqs. (4) and (5)). The E_M also is proportional to the applied electrical RF power.

Importantly, the *sensitivity* of a "copper only *detector*" (right part of Fig. 1) for a longitudinal ultrasound vibration (infinite plane wave) is not – as in Eq. (6) – an integral of the squared magnetic energies. Instead, just the integral of energies is required, as already known for conventional EMATs [2].

Eq. (6) is a nonlinear (squared energies) specialty for an EMAT *transducer* without a static field. It has significant influence on the geometric design rules – including an efficiency optimum – for such transducers, and therefore, justifies these considerations.

A quite related equation (instead of Eq. (6)) could also be derived for conventional EMATs with separated B_{RF} (from a concentric RF coil) and B_0 (e.g., from a coaxial and stationary magnet, like shown in [12]), which also would allow rather detailed insight and potential optimization rules. For these conventional EMATs the obtained B_{RF} (from Eq. (2) *with* mirror coil) can be used for the eddy current field in the metal (Eq. (3a)) and the separately determined B_0 (e.g., from Eq. (2) *without* mirror coil) then can be used for the Lorentz forces (similar to Eq. (3b)).

In the "pancake coil" (axial symmetry) geometry described above, the profile of the acoustic pressure appears as a diffuse ring on the surface. The pressure only depends on r and not on the angular position; the field energy is distributed uniformly over 360°.

An interesting question for maximizing acoustic power A in relation to available electrical energy E_M would be whether the pressure or energy density p can be *concentrated* in a certain angle position and *reduced* for all other angles. Under this assumption, with the same amount of total energy E_M in the system, acoustic power could be higher than from an ordinary pancake coil, due to the nonlinear behavior of the acoustic intensity (proportional p^2 or B^4, Eq. (6)). In addition, with an effectively smaller acoustic footprint, potentially smaller targets or target areas could be addressed, not with an acoustic ring pattern, but with a more spot-like excitation.

In general, this idea tries to combine the advantage of a small coil (higher field concentration → higher conversion efficiency) with that of a larger coil (more range). Fig. 2d shows a concrete sketch of this idea, commonly known as a "butterfly coil." In this design, the majority of the magnetic energy and inductance is located around the five narrow, parallel, and linear wires (compare [4,5,16]: "linear coil") in the center. The wider wings of this "butterfly" carry a significantly lower current density (about 1/5), and thus, a much lower magnetic energy density (about 1/25). As a result, the concentrated wires in the center should obtain about five times more inductance per length than the wings. Here, it is estimated that about 60–70% of the inductance (=field energy) is localized at this dense center.

A possible advantage of the butterflýs dense center over a pancake coil with a similar area (or density) is the higher reach: in the butterfly coil, the currents in the dense center are all *unidirectional* and *parallel*; in constructive interference, they all induce the same magnetic effect in the target (i. e., a contra-directional eddy current). Conversely, a pancake coil carries *circular* currents and, following the idea of the Biot–Savart law, the effect of each current element is weakened by a contra-directional current element from the other side (180° angle position). Actually, at the center axis of a pancake coil, the induced eddy current is zero, even for very close targets: at this point, all current elements compensate each other for the radial field component. From destructive interference, the pancake coil produces an acoustic "hole" in the center; therefore, the pressure profile is a diffuse ring, even for high filling ratios f/R. This destructive interference also affects the reach of the circular pancake coil.

The center axis of the butterfly coil would be the point of maximum eddy current and maximum pressure; only constructive interference is obtained from the dense center. When comparing the circular area of a pancake coil with this "hot area" of the butterfly coil, it is assumed that for comparable areas and comparable energies, the butterfly coil probably yields more reach. This is of practical interest. Indeed it is already well known for completely other application fields (electromagnetic brain stimulation, Transcranial Magnetic Stimulation (TMS)), that the field of butterfly coils is more focused and concentrated in comparison with the circular coils [17]. Also, for *conventional* EMAT designs (with stationary field/permanent magnet) it is already shown, that a butterfly coil design can generate stronger induced currents and higher Lorentz force densities in the test specimen, and then it is somewhat less sensitive to the effect of lift-off [18]. This advantage could become even higher for the herein discussed *unconventional* EMATs without stationary field, since the transmitted ultrasound intensity scales with B^4, not only with B^2.

As a further remark, a butterfly coil is, due to the symmetric geometry (Fig. 1d), significantly less sensitive for electromagnetic interference from external sources: sensitive detection of small signals is improved. This advantage is mentioned and patented by the manufacturer NORDINKRAFT Corporation for conventional EMATs with stationary field.

2. Numerical and experimental methods

Eqs. (2), (4), and (6) were implemented in a MATLAB® (The MathWorks, Inc.) script. The space was discretized and limited to a finite volume around the coil; the considered volume was chosen to contain most of the coiĺs magnetic energy E_M.

For comparison purposes, a FEM computer simulation in COMSOL Multiphysics®—as presented in previous contribution [9]—was carried out. The FEM simulation only approaches (as in nature) the fulfillment of Maxwelĺs equations in every point of the space; it is not a straightforward calculation and it does not implement the above equations or considerations. Some FEM results are shown in the supplement; they were just used for confirmation (besides experiments) of the analytical calculations.

Fig. 3 is a cross-sectional view in the r–z-plane. It shows quantitative field calculations based on the above equations. The flux densities B in space—resulting from coil currents and eddy currents—are displayed in intuitive colors. The geometries and currents were chosen in a way that most fields are lower than 1 T. Here the discretization is chosen as 1 mm. The results of this straight forward method are quite insensitive to the discretization scale, as long as the general geometries of the scenario are reasonably wider (exception: δ can be much smaller, is not involved in this calculus).

Fig. 3a–c shows a single and circular current loop with $I = 10$ kA and radius $R = 20$ mm in free space, center point at $r = 0$ and $z = 11$ mm. The characteristic cross-section of the wire then – due to 1 mm discretization in this calculation – would be just 1 mm^2. Fig. 3a is the total flux density, Fig. 3b the flux density B_r in radial direction (from Eq. (2a), negative sign suppressed) and 3c the flux density B_z in axial direction (Eq. (2b), negative sign suppressed). When positioning a (non-ferromagnetic) metal block at $z < 0$ and using a DC current for a stationary field, the presented field topology would not change. In principle, field topologies from permanent magnets or quasi-stationary electromagnets can be approached by a suitable arrangement of such current loops.

The same current loop with 10 kA is shown in Fig. 3d (total flux density), e (radial component B_r) and f (axial component B_z), but now an RF current and a well conducting metal plane (here: $\delta \ll 1$ mm) at $z = 0$ is implied. Thus, $g = 10$ mm. The eddy currents in the metal's skin sheet would deform the field. Virtually the same deformation is obtained by a mirrored current loop at $z = -10$ mm and this is actually done here. Now the radial field component B_r close to the metal (Fig. 3e) is doubled ("field compression") and the axial field component B_z near the metal (Fig. 3f) is nulled. The "technical data" of the scenario Fig. 3d–f is as follows: the overall force onto the metal plane is 71 N (by integration of magnetic pressure at $z = 0$) and the total energy E_M of the field was integrated within $0 < z < 30$ mm and $0 < r < 40$ mm (Eq. (3)) to 3.8 J. Then, from Eq. (4), the inductance L of the loop – a 1 mm wire, 4 cm diameter and 1 cm above a metal plane – becomes 76 nH. The influence (axial distance g) of the metal sheet onto inductivity can be well studied with this method, similar to [6]: toward smaller g the inductance L significantly decreases. The practical inductance (experimentally by LC-resonance) of such a wire loop is close to 80 nH.

Fig. 3g shows a superimposition of 10 concentric RF current loops, each carrying 1500 A and positioned over a metal plane. The scenario represents the dynamic field of a pancake coil with $R = 20$ mm, $f = 10$ mm and $g = 10$ mm. The total force onto the metal is 91 N and the total field energy is 3.5 J. The "efficiency" (here just force over energy) is higher than for Fig. 3d, since in 3d stronger fields (>1 T) occur close to the single wire. The inductance in Fig. 3g would be much higher, namely 3 μH. This is simply caused by 10 windings instead of just 1 winding in Fig. 3d.

It is assured that this analytical model quite reasonably describes the experimental findings of previous contribution [9]. For $E_M = 8$ J, $R = 7$ mm, $f = 2$ mm and $g = 1$ mm indeed a force of 4.8 kN and an acoustic power of 1.2 kW (Eq. (6)) for aluminum metal can be calculated. In [9] a force of ≈4.5 kN (from magnetic pressure, independent from metal type, even for ferromagnetic iron or steel) was experimentally observed, and an acoustic power of somewhat more than 1 kW was proposed for aluminum.

Physical laboratory experiments: As already described in much more detail and readily available for the interested reader [9], a 150 nF capacitor (Fig. 1, left part) with low serial inductance (all elements included result in about 90 nH) was charged to 16 kV,

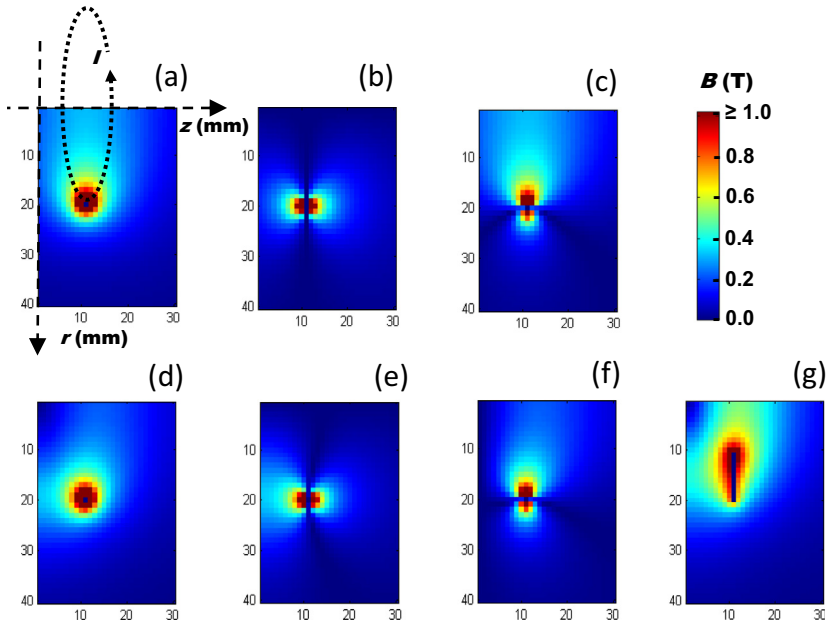

Fig. 3. Analytical field (Eq. (2)) of a current loop at 10 kA. (a) Total field amplitude, (b) radial field component, (c) axial field component. (d–f) Same current loop with mirror coil (placed at $z = -10$ and not visible here), representing an RF field over a metal plane at $z = 0$. (d) Total field amplitude, (e) the radial field component is increased toward the metal plane, (f) the axial field component is nulled close to the metal plane. (g) 10 current loops at RF frequencies over a metal plane, modeling a situation similar to Fig. 2b: a pancake coil with certain R and f.

and it then contained 17 J electrical energy. The capacitor was able to discharge very quickly over a switch (low inductance/low resistive spark gap, already included in the 90 nH) into the transducer coil. For an LC-oscillation frequency of 1 MHz, the total inductance should be 180 nH, and therefore, only 90 nH remain for the transducer coil. Then, an electrical energy of about 8 J was converted into magnetic energy E_M in the coil, and the oscillating currents approached 14 kA (Eq. (5)). Non-contact ultrasound signals (at doubled frequency: 2 MHz) were excited in an aluminum rod 3 cm in diameter (used as a delay line), and the sound could be detected with a conventional and strongly damped – for bandwidth – piezo element (instead of the EMAT receiver in Fig. 1) at the right end of the delay line. The squared amplitude of the piezo signal was interpreted as proportional to the ultrasound power A. Naturally, with the more complex mode structure in the signal [9,10] and that mode structure depends on the pressure footprint (which itself depends on g) of the transducer [14,15], this method for relative power metering is just an experimental approximation. Nevertheless, the required accuracy for relative power metering is not very high, since the actually relevant power effects extend over orders of magnitude. The transmitter coils, with relatively few windings, were handmade from conventional copper wire. Achieving reliable electrical insulation and mechanical rigidity of the individual windings were delicate processes that posed some problems. Thermal problems were not a predominant concern, due to the low repetition frequencies, a cooling fan and sufficient coil sizes.

3. Results

Fig. 4 shows the acoustic amplitudes (experimental data: piezo signal in volts) from two different coils as a function of g. The two coils acted on aluminum metal. The effective acoustic power A in the aluminum is believed to be proportional to the square of these electric amplitudes. The experimental data was copied from a previous contribution [9]; the diameters of those pancake coils were 1.5 and 2.4 cm. At small distances g, the smaller coil provided more

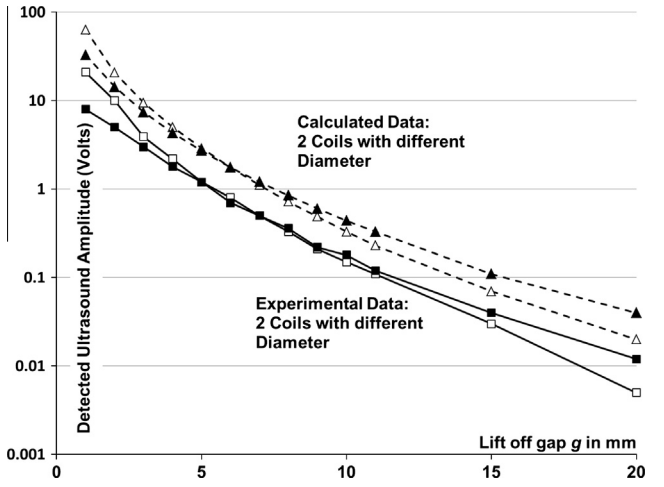

Fig. 4. Experimental ultrasound amplitudes (piezo raw signal in V) at 2 MHz over distance g from a small coil (white squares) and larger coil (black squares). Experimental data was copied from [9]. The calculation (Eq. (6), triangles) of coils with similar geometries results in quite similar behavior over distance. The calculated data are shifted upwards for a better representation, as there is not a measurable signal.

acoustic power and the energy was more concentrated. At higher distances, the larger coil ultimately became more efficient, as it attained further reach. Maximum power was achieved for the smaller coil, and at $g = 1$ mm, that power was estimated to be close to $A = 1.2$ kW.

As a comparison, two coils with $R = 9$ mm (four narrow windings with 1 mm wire, $f = 4$ mm) and $R = 12$ mm (two individual windings, separated by 3 mm) were quasi-analytically computed on the basis of the above equations. At $g = 1$ mm, the smaller coil was computed to deliver $A = 1.1$ kW for 8 J energy. In contrast, the larger coil only provided $A = 330$ W for the same excitation energy. The calculated point "1.1 kW" was normalized to an amplitude of "65 V" in the graph, as it was not a measurable value for the

piezo detector. The distinct offset for the calculated data provides a better presentation, rather than overlaying all calculated and experimental data.

Besides all uncertainties (difficulty of exactly determining the total magnetic energy at RF frequencies in the transducer, usage of a simplified calculation for acoustic power (Eq. (6)) and piezo amplitude instead of analyzing complex acoustic fields and mode structures [9,10,14,15], or practical geometries: a handmade coil with only two to three thick windings in a spiral and with the required connecting wires will not behave exactly like a number of concentric current circles) a quite reasonable match (slope, crossing) can be stated between the experimental results and the calculated data, much better than discussed and shown in [9] with the simplified description. Although including some approximations, the mathematical model appears to be a quite useful tool for modeling and optimizing such coils.

The graph suggests that for each g and for a limited energy E_M, an optimal geometry of a pancake coil (R and f) as a transmitter (not as a receiver!) might exist for a maximum acoustic power A. Fig. 5 shows the calculated acoustic power A into an aluminum plane at a quite considerable g = 10 mm and E_M = 8 J for very different coil diameters R and different filling f (f must be smaller than R). Within filling f, dense windings without separation are assumed (like presented in Fig. 3g).

For small R (starting at 5 mm) and small f, the energy is concentrated at the very local coil environment, and it does not effectively extend to the target, therefore, the acoustic response is poor. Toward higher R, the acoustic signal increases rapidly and a maximum appears at about R = 30 mm. Toward even higher R, the acoustic power gradually decreases. Although the larger coils reach the target better, the dilution of energy density in space accounts for the decrease: nonlinear response in Eq. (5). An oversized coil (R > 30 mm), however, seems to be less critical than an undersized coil (R < 30 mm).

Furthermore, the relative high fillings f yield maximum transmitter efficiency for the pancake coils. High filling reduces energy density at the coil plane, and more energy is available at the target plane. For very oversized coils, however, a high f further dilutes the energy density at the target site, and the acoustic output decreases (see distinct point at R = 100 mm and f = 90 mm).

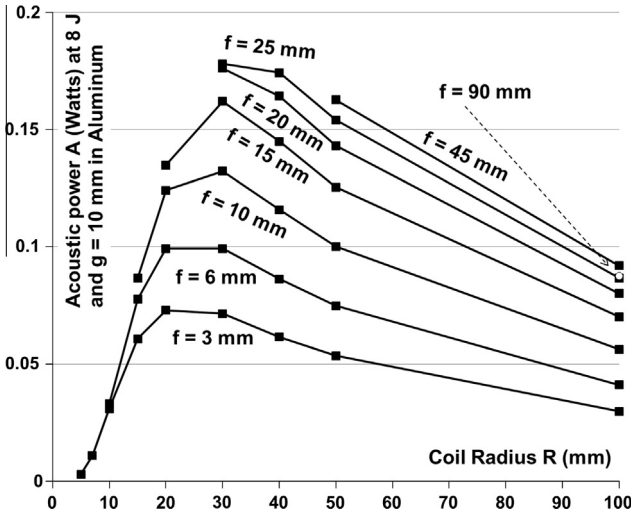

Fig. 5. Obtained ultrasound power A from various pancake coil sizes at a given energy of 8 J and a given distance of 10 mm (calculation). Small "undersized" coils are not effective. The optimum appears around R = 30 mm and high fillings f. Toward "oversized" coils, the output decreases again due to the dilution of energy density in space. For very oversized coils, a high filling further decreases the energy density, and therefore, the efficiency falls off even more (distinct point for R = 100 and f = 90).

For technical reasons, a relatively small radius of the inner windings or a high f/R should be avoided. As a more generalized rule for optimum design of this transmitter principle, $R \approx 3\ g$ and $f \approx 2\ldots2.5\ g$. For *receiving* signals of a homogeneous plane wave in the metal, a different rule applies: the R simply should be as wide as possible to provide a virtually homogeneous field in the gap and almost no field energy outside the gap. The non-linearity of Eq. (6) exclusively accounts for transmission and not for receiving ultrasonic signals.

For g = 1mm and at 8 J, an optimized transmitter coil (R = 3 mm, $f \approx$ 2 mm) is calculated to 1.8 kW acoustic power in aluminum, not only 1.1 kW as calculated above (Fig. 4) with R = 9 mm. It then must be noted that in such small geometries, the pressures and Lorentz forces at 8 J easily exceed 1000 atmospheres, or 20 T. A practical coil probably cannot withstand such mechanical and electrical stress at RF frequencies. At sufficiently smaller energies, however, it should not be a problem.

As a general remark, an optimized coil (R = 3 g), and particularly even more oversized coils as receivers, are relatively large: a coil diameter of 6 cm or even more—optimized for just a 1 cm reach—is not attractive for every application. One obvious reason might be that the target area itself is smaller than 6 cm, such as the 3 cm target area of the experimental aluminum rod described earlier. Another reason could be that the acoustic footprint and the acoustic beam inside the target become too wide for a reasonable resolution in nondestructive testing.

Therefore, it is interesting to investigate alternative geometries, as illustrated with the butterfly coil in Fig. 1d. The evolution of a butterfly coil from a pancake coil is shown in Fig. 6; the magnetic and acoustic (acoustic power density) footprints in the target area (z = 0) from different coil geometries at g = 1 mm and g = 5 mm are presented with qualitative color coding. The applied energy E_M or electric power is fairly the same for the different geometries at g = 5 mm.

The normal pancake coil (five *concentric* windings) in the first row produces a ring as a magnetic and acoustic footprint. At higher liftoff (g = 5 mm), the ring becomes more diffuse, and the patterns from the individual windings disappear, as expected from the cross-sectional views in Fig. 3.

When modifying the coaxial pancake coil toward five *excentric* windings, as shown in the second row, the field intensity concentrates at the upper part (12 o'clock) and is relieved at other angles (3–9 o'clock). The acoustic footprint, being proportional to B^4 in transmitter mode, is then concentrated in a relatively small area around 12 o'clock. The other angles almost disappear with the acoustic effect. At higher liftoff (g = 5 mm), the local concentration is still observable, although the effect notably blurs over the distance in space.

In the third row, a second excentric pancake coil is superimposed in such a way that the dense areas constructively overlap. Now, the magnetic field intensity, and particularly the acoustic footprint, is significantly increased in this "hot spot." For all other positions, the acoustic contribution seems to be almost negligible. Such a relatively smaller and focused acoustic footprint, without a central void and even present at a higher distance, might be attractive for practical applications. A relevant question is whether, for such geometries, besides the transmitted acoustic *power density* being locally enhanced as a benefit of the nonlinear relation, the *total acoustic power A* is higher or at least comparable to an ordinary pancake coil.

Because no axial symmetry is present in more complex geometries, a simple two-dimensional calculation in the r–z-plane is not sufficient anymore. The problem must be considered as three-dimensional, and Fig. 6 is calculated in Cartesian coordinates x, y,

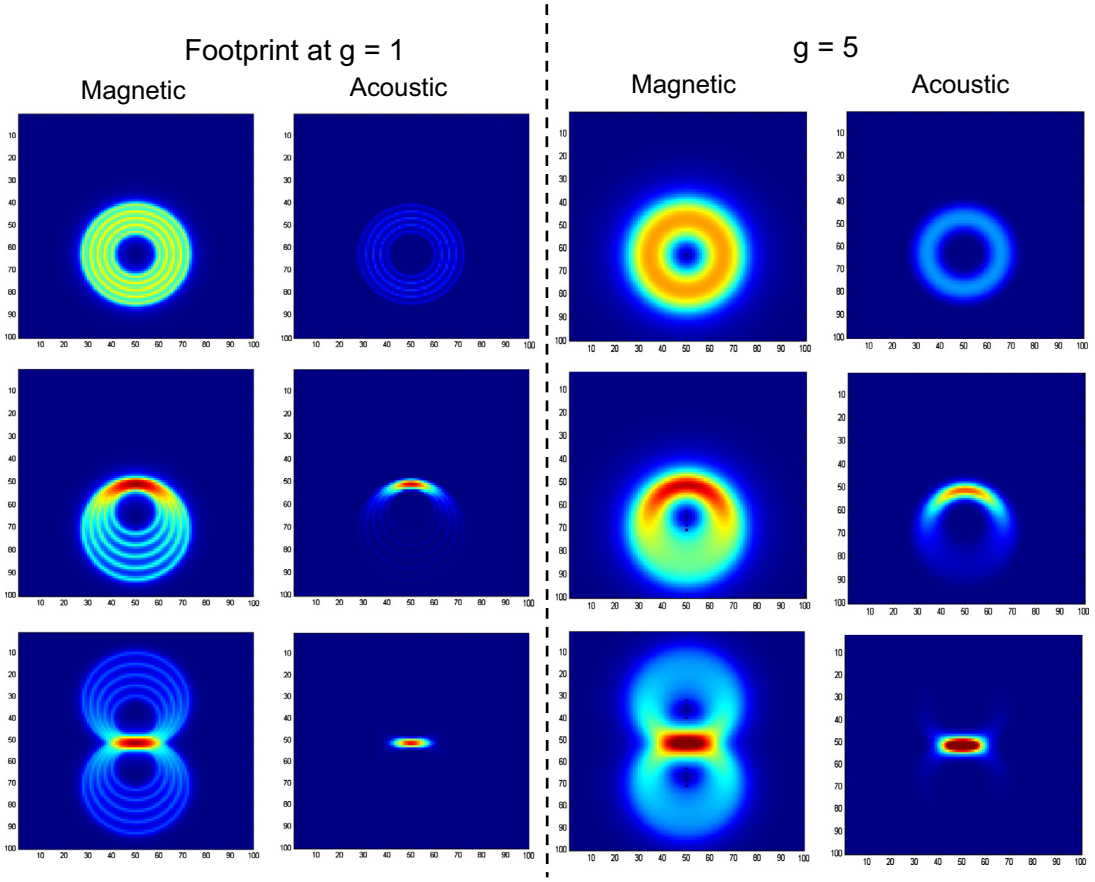

Fig. 6. Evolution of a butterfly coil from a circular, concentric pancake coil. All views in the target plane, at $z = 0$ mm. The magnetic and acoustic footprints from a normal pancake coil are shown in the first row. For $g = 5$ mm, the appearance of the magnetic and acoustic footprints becomes more diffuse, and a characteristic ring appears as the acoustic footprint. In the second row, the pancake has become excentric and the fields and acoustic effects are concentrated in the upper parts with high density. In the third row, an additional excentric pancake is superimposed in a way that that the concentrated parts are even more enhanced. A more spot-like footprint appears and the acoustic density is significantly increased, even over some distance ($g = 5$ mm). The total energies for the three different arrangements at $g = 5$ mm are fairly equal.

and z. The individual field components of the loops in the r-direction had to be converted into x-components and y-components first. Then, the multiple loops with fields in Cartesian coordinates could be superimposed.

From a numerical integration (in Cartesian coordinates, similar to Eq. (6)), it was found that in Fig. 6, for the same total energy E_M, the coaxial pancake coil ($R = 22$ mm, $f = 12$ mm) at $g = 5$ mm still delivers 2.5 times more acoustic power than the butterfly arrangement with the "hot spot." The acoustic power density in the "hot spot" is already much higher than in the diffuse ring from the pancake. To the benefit of the butterfly, it should be noticed that the pancake coil is already not very far from an optimum geometry (Fig. 5) for $g = 5$ mm; on the other hand, the demonstrated butterfly coil with the "hot spot" is still not optimized at all. A butterfly principle with a more optimized geometry could finally close up or even outperform the acoustic power of a pancake coil.

A weakness of the butterfly presented in Fig. 6 is that the created "hot spot" (the acoustically active zone) from the two excentric pancakes is much shorter with respect to the total circumference of the coils (the acoustically passive zone, but it is still inductive and demands energy). This geometric disadvantage simply results from the mathematical circles in Fig. 6. Although the circles could be mathematically stretched into ellipses with a relative longer overlap at the "hot zone," the fundamental problem would persist, due to the stretching of all other geometries.

In comparison, the butterfly sketched in Fig. 1d has a longer "hot zone" (five central wires) with respect to the wide back wings (only two wires each side), which is readily achieved by using straight, parallel lines (see calculation in supplement paragraph 7: "Two-Wire-EMAT") instead of mathematical arcs with different curvatures and orientations.

Therefore, in an experimental trial, two circular pancake coil and a linear butterfly coil were experimentally designed for the application $g = 5$ mm. The experiments were carried out with an aluminum rod with a 30 mm-diameter target area, as already described in [9] and similar to Fig. 1.

The design for the pancake coil is quite easy now: $R = 3 * 5$ mm leads to a 30 mm-diameter coil. The filling f should be high, about 12 mm. Actually, the coil could not be larger, as the target itself is limited to a diameter of 30 mm. A pancake coil that was any larger would probably not help here anymore. It would only be useful in an excentric geometry; however, this ultimately results in the butterfly concept (evolution in Fig. 6).

In the practical experiments, coils with $R = 14$ mm (28 mm diameter) and $R = 8$ mm were handmade and tested; they were similar to but not exactly the same as shown in Fig. 4 from the older experiments.

For the butterfly with more describing geometries, the uncertainties for a suitable design are much higher. Nevertheless, the active width was chosen as $w = 5$ mm (Fig. 2d) and the lateral distance to the back wing was 15 mm. The active length L should be longer than the "hot zone" in Fig. 6, to accommodate relatively more energy in this acoustically active part. Furthermore, length L should be higher than lateral distance 15 mm to accommodate

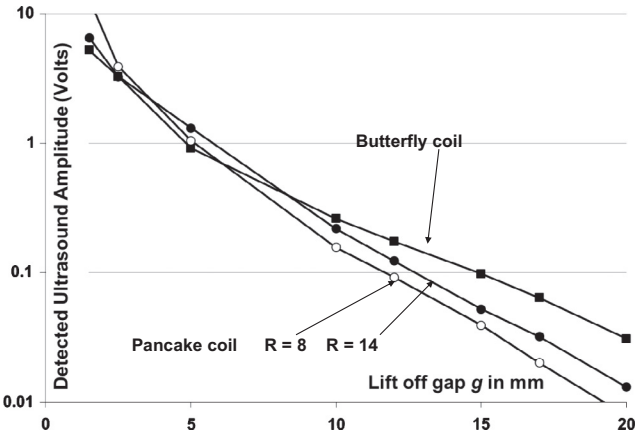

Fig. 7. Transmitted signal amplitudes from practical butterfly compared with practical pancake coils (28 mm diameter and 16 mm diameter, similar to Fig. 4); target area is 30 mm-diameter aluminum. At greater distances g, the butterfly is clearly superior and delivers about five times the signal power (=squared amplitude) at $g = 20$ mm.

sufficient inductance in the central strip with respect to the necessary ways in the lateral direction. Therefore, length L uses the full size of the target and becomes 30 mm.

From experimental findings, only three wires were taken for the central strip (not five as sketched in Fig. 2d), and only two solid back wings were required (not four as in Fig. 2d). Then the total inductance became 150 nH and this fairly matches the experimental requirements.

Fig. 7 shows the experimental results as acoustic amplitudes in the piezo signal, obtained in volts as the 2 MHz raw signal. The two circular pancakes behaved in a very similar manner as shown in Fig. 4. The circular $R = 14$ mm coil was slightly more powerful at $g = 5$ mm and at higher distances, as already discussed. At shorter distances, the $R = 8$ mm coil became more powerful due to the higher field density. The practical butterfly coil was not superior at small distances; it only approached the $R = 14$ mm coil. However, the butterfly became more effective at higher distances above 10 mm: At $g = 20$ mm, about five times the acoustical power (=squared amplitude) was obtained experimentally than from the larger circular coil. This is a quite significant improvement and not just caused by different mode structures in the rod. Notably, distance g affected the butterfly's signal less, as the slope was less steep. In addition, the butterfly coil produced a smaller footprint than even the smaller circular coil.

The characteristic footprint can be visualized practically with malleable aluminum foil as a target material: the magnetic pressure of a pancake prints a characteristic toroid (with a non-affected center) in the foil, similar to the diffuse rings shown in Fig. 6. The butterfly produces a linear ditch over length L, almost as if impressed by a sharp edge and naturally without a passive center. Undoubtedly, then, the acoustic beam propagation inside the target will also differ: due to diffraction [14,15], the opening angle would be smaller when parallel to the magnetic "blade" in the L-direction and higher in the perpendicular w-direction (Fig. 2d).

From the viewpoint of efficiency, the butterfly appears to be clearly superior when trying to affect relatively small metal targets over a distance. The range of a butterfly seems to behave like an "oversized" pancake coil; nevertheless, it can "focus" better on a relatively small target area over some distance.

4. Conclusion

Simple induction coils can be used as non-contacting transducers and detectors for ultrasound in metals. An EMAT without a voluminous stationary magnet could be of practical interest. Another interesting feature could be the potentially stronger dynamic fields and these are even in inherently good overlap to eddy currents. This could help to gradually increase the electroacoustic efficiency (more powerful transmission and more sensitive detection) of EMATs. The analysis and straight forward calculation of magnetic field topologies with a simplified computer model reasonably describes the acoustic intensities of concentric pancake coils as ultrasound transducers; it allows predictions and an optimization for such geometries. The presented calculus might also be altered and then readily applies to conventional EMATs, with separate RF and DC fields.

For somewhat lower energies (probably a more practical approach: then based on solid-state switching and suitable for high repetition frequencies) and lower field intensities, the use of ferromagnetic materials, like iron powder cores or ferrite, as back plates should be advantageous. This was already presented by Jian and Dixon [7]. As an appreciated feature, for simple induction coils as an ultrasonic transmitter and receiver, such a back plate would not interfere with the field of stationary magnets (as required in conventional EMATs).

The partly superior butterfly concept with more and more complex geometries currently was not fully accessed with quasi-analytical methods. However, it was shown experimentally that the butterfly, with a more dense and linear center, could be advantageous for the very practical problem of "relatively small target areas at a certain distance". It is believed that when experimentally verified, a more extensive and detailed modeling of the various butterfly geometries will ultimately result in better performance of EMAT transducers and receivers for the technically interesting scenario "targets at a certain distance".

Acknowledgements

This work is initiated and supported by the internal research founding of the University of Applied Sciences Ruhr-West. The author wishes to thank Tino Morgenstern [9] for performing the FEM crosschecking.

Appendix A. Supplementary material

Supplementary data associated with this article can be found, in the online version, at http://dx.doi.org/10.1016/j.ultras.2015.10.003.

References

[1] H.M. Frost, Electromagnetic-ultrasonic transducers: principles, practice and applications, in: W.P. Mason, E.N. Thurston (Eds.), Physical Acoustics, vol. XIV, Academic Press, New York, 1979, p. 179.
[2] E.R. Dobbs, J.D. Llewellyn, Generation of ultrasonic waves without using a transducer, Non-destruct. Test 4 (1971) 49–56.
[3] K. Kawashima, S. Murota, Y. Nakamori, H. Soga, H. Suzuki, Electromagnetic generation of ultrasonic waves in absence of external magnetic field and its applications to steel production lines, in: Proc. 9th World Conf. on Non-Destructive Testing, vol. 4H–3, 1979, pp. 1–8 [11].
[4] M. Hirao, H. Ogi, EMATs for science and industry, Noncontacting Ultrasonic Measurements, Springer, 2003.
[5] X. Jian, S. Dixon, R.S. Edwards, Modelling ultrasonic generation for Lorentz force EMATs, Insight (BINDT) 46 (2004) 671–673.
[6] X. Jian, S. Dixon, R.S. Edwards, J. Morrison, Coupling mechanism of an EMAT, Ultrasonics 44 (2005) e653–e656.
[7] X. Jian, S. Dixon, Enhancement of EMAT and eddy current using a ferrite backplate, Sens. Actuators, A 136 (5/1) (2007) 132–136.
[8] J. Krautkrämer, H. Krautkrämer, Ultrasonic Testing of Materials, fourth fully rev. ed., Springer-Verlag, Berlin, New York, 1990.
[9] D. Rueter, T. Morgenstern, Ultrasound generation with high power and coil only EMAT concepts, Ultrasonics 54 (2014) 2141–2150.
[10] J.R. Hutchinson, C.M. Percival, Higher modes of longitudinal wave propagation in thin rods, J. Acoust. Soc. Am. 44 (5) (1968) 1204–1210.

[11] C.V. Dodd, W.E. Deeds, Analytical Solutions to Eddy-current probe-coil problems, J. Appl. Phys. 39 (1968) 2829, http://dx.doi.org/10.1063/1.1656680.
[12] K. Kawashima, Theory and numerical calculation of the acoustic field produced in metal by an electromagnetic ultrasonic transducer, J. Acoust. Soc. Am. 60 (1976) 1089–1099.
[13] R.H. Good, Elliptic integrals, the forgotten functions, Eur. J. Phys. 22 (2001) 119–126.
[14] S. Takahashi, On the sound field of a plane radiator with an arbitrary contour shape, Acustica 44 (1980) 336–338.
[15] W.J. Pardee, R.B. Thompson, Half-space radiation by EMATs, J. Non Destr. Eval. 1 (1980) 157–181.
[16] R.B. Thompson, A model for the electromagnetic generation and detection of Rayleigh and lamb waves, IEEE Trans. Sonics Ultrason. vol. SU-20 (4) (1973) 340–346. herein Eq. (15).
[17] L.G. Cohen, B.J. Roth, J. Nilsson, N. Dang, M. Panizza, S. Bandinelli, W. Friauf, M. Hallet, Effects of coil design on delivery of focal magnetic stimulation. Technical considerations, Electron. Clin. Neuro. 75 (1990) 350–357.
[18] E.C. Ashigwuike, W. Balachandran, S. Thomas, R. Mackay, Numerical study of EMAT coil structure based on finite element method, Petrol. Technol. Dev. J. 3 (1) (2013).